FULL LENGTH PAPER

CONJUGATE HEAT TRANSFER ANALYSIS OF SCRAMJET COMBUSTOR

Anand Bhandarkar; Malsur Dharavath; P. Manna; Debasis Chakraborty
Directorate of Computational Dynamics
Defence Research and Development Laboratory (DRDL)
Kanchanbagh Post, Hyderabad-500 058
Email : debasis_cfd@drdl.drdo.in; debasis_drdl@yahoo.co.in

Abstract

Conjugate Heat Transfer (CHT) simulation with reacting flow in scramjet combustor is performed. Three dimensional RANS equations with k-ω turbulence model, EDM combustion model for fluid domain and energy equation in the solid domain are solved simultaneously using commercial CFD software. The SCHOLAR scramjet combustor experiment is taken as a test case of validation. The computed flow properties match reasonably well with experimental data and other numerical simulations. Near fuel injection locations, computed surface temperatures over predict experimental data due to use of fast chemistry for combustion modeling. In the downstream, at the diverging section of the combustor, computations under predict the surface temperature. Use of natural convection boundary condition is found to have marginal effect in the surface temperature history of the scramjet combustor. Temperature dependent material properties are found to have significant effect in the distribution of temperature across the combustor wall.

Keywords: *Conjugate Heat Transfer, Scramjet, CFD, High Speed Reacting Flows*

Introduction

The goal of heat transfer studies is the accurate prediction of temperature and heat flux distribution in time and space in a body and on its boundaries. One of the most interesting problems that arise in heat transfer studies are when the solid body is immersed in a fluid flow and its walls are thermally conductive. In the past, it was common to simplify the problem by calculating first the flow field and then evaluating the temperature inside the solid body separately by imposing a prescribed wall heat flux or temperature at the interface. This could be acceptable for some applications but it neglects the physics of the problem, in which there is an active coupling between the aerodynamic flow outside the body and the thermal field inside it. For such an interaction between heat conduction in the solid with convective heat transfer in the fluid, Conjugate Heat Transfer (CHT) problem needs to be solved. CHT problems are found in many real life applications including turbo-machinery, re-entry vehicles, heating ducts and scramjet combustor applications etc. Accurate modeling of convective heat transfer in the fluid and conductive heat transfer in the solid is required for CHT problem simulation. Due to increased speed and memory storage of modern computers, improved computational schemes as well as grid generation algorithms, this problem is currently amenable to numerical simulation.

CHT capabilities of commercial codes were explored by Manna and Chakraborty [1] for low speed laminar flow over a flat plate and turbulent flow between two parallel plates and obtained good match between the computed and experimental temperature and heat transfer coefficient. Chandramurty et al. [2] studied Conjugate heat transfer problems for high speed flows including laminar flow past axisymmetric double cone at Mach 4.57 and turbulent flow past circular cylinder at Mach 6.7. Computed skin temperature history shows a good match with experimental, flight measurements and other numerical results. Marineau et al [3] validated conjugate heat transfer capability of the GASP flow solver [4] against many test cases including a water-cooled supersonic nozzle flow experiment of Back et al. [5] and obtained good agreement between computed and experimental data. Aydin et al. [6] studied laminar conjugate heat transfer problem in a tube

Paper Code : V68 N4/932-2016. Manuscript received on 11 Dec 2015. Reviewed, revised and accepted as a Full Length Contributed Paper on 16 Aug 2016

with axially varying heat flux at the outer wall and estimated the effects of thermal conductivity ratio, diameter ratio and periodic heat flux on local and mean Nusselt numbers, temperature and the interface heat flux distribution. Engblom et al [7] introduced the conjugate heat transfer capability of general purpose CFD code WIND [8] and TBD [9]. The computations were validated against water cooled supersonic flow experiments of different nozzles and panels. Requirement of more sophisticated treatment of water coolant heat transfer mechanisms of convection and boiling was recommended for better agreement between experiment and computation. Mathew and Davis [10] introduced the CHT capability in Detached Eddy Simulation (DES) code [11] and studied the effect of Reynolds numbers on surface temperature of unsteady flow past circular cylinder.

Although, Computational Fluid Dynamics (CFD) codes are extensively employed in the design of high-speed air-breathing engines, the application of CHT techniques in high speed internal flows are not many. Designers are still applying the separate methods of fluid flow and heat transfer methods in analyzing high speed internal flows. Chandramurty et al. [12] has solved SCHOLAR [13-15] scramjet combustor flow field and thermal response of solid walls separately. Eckerts reference temperature method (engineering correlation) and CFD predicted heat transfer coefficients for different wall temperatures were used for thermal analysis of combustor wall. Although, experimental trends of surface temperature were captured, there exist significant differences in computed and measured values. Rust et al. [16] studied the surface temperature distribution of a fuel injection strut placed in the flowpath of a hydrogen fuelled scramjet combustor and provided boundary and injection conditions for further flow calculation in the scramjet combustor. CHT analysis with reacting flow has not been reported adequately in the open literature. In practical applications, combustion of fuel causes significant heat load to scramjet combustor inner walls and aerodynamic heating due to external hypersonic flows contributes to outer walls heating. Accurate prediction of wall temperature (which can be obtained through CHT analysis of reacting flow) is required to select the material and thickness of the combustor. In the present work, CHT analysis of the SCHOLAR scramjet combustor is carried out using a commercial CFD solver CFX-14 [17] and the computed flow and wall temperature data are compared with experimental data.

Description of the Experiment for which the Simulations are Carried Out

To validate CFD data, a focused experiment of a model scramjet combustor (SCHOLAR) was conducted at NASA Langley's Direct-Connect Supersonic Combustion Test Facility [13-15]. Hot air stimulant (vitiated air) is produced in a hydrogen based heater. Flow rates are adjusted in such a manner, that the mass fraction of oxygen in the vitiated air is same as that of atmospheric air. The high pressure, hot vitiated air is then accelerated through a water-cooled convergent-divergent nozzle, before entering into the combustor test model. The facility nozzle is designed to provide a nominal Mach number of 2.0 at the entry of the combustor. Hydrogen fuel is injected at 30° angle into airstreams with 1200 K temperature in a divergent duct. The enthalpy of the test gas (vitiated air) is equivalent to Mach 7.0 flight. Detailed measurement of temperatures and species mole fractions at various cross sections using CARS thermometer and wall pressures are used to understand the progress of mixing and reaction in the combustor. The forward section of the combustor is made of copper while the rearward portion (divergent section) is made of carbon steel. Measurements of temperature histories at three different axial locations at the top wall of copper and carbon-steel sections provide very good data for validation of the code.

The combustor test model along with the facility nozzle is shown in Fig.1. Flow direction is from left to right as shown in the figure. The combustor consists of two main sections of duct: the copper upstream section and the carbon steel downstream section. Stainless steel flanges and carbon gaskets separate the sections from each other and the nozzle. The wall thickness of the copper and carbon steel ducts are 32 mm and 19 mm respectively. Proceeding from left to right, there is a constant area segment, a small outward step at the top wall, a second short constant area segment followed by a constant 3° divergence of the top wall. The bottom wall is flat and horizontal. The span is constant at 87.88 mm. The height (H) of the combustor at entry is 38.86 mm while the height at the exit is 112 mm. Five small pilot fuel injector holes are located ahead of the step in the top wall, and the main fuel injector is located just downstream of the start of the 3° divergence. The injection angle is 30° to the opposite wall. The injector nozzle is designed by the method of characteristics to produce Mach 2.5 flow at the injector exit. Hydrogen injection is provided at a pressure of 3.44 MPa and temperature of 302 K, with the equivalence ratio of about 1.0. Although, the duct is uncooled, large thick-

ness and good thermal conductivity of materials, it is possible to operate the facility in excess of 20 s.

The model is instrumented with both pressure taps and wall temperature probes. Pressure taps are located at the bottom wall centreline. Temperatures are measured at 3 locations in the top wall, two in copper block and one in steel block. K-type thermocouples are used to measure solid temperature. The thermocouple probe material is made of carbon-steel predominantly. In the copper block, thermocouple probes are located inside the solid at 2.8 mm above the interface, whereas, in the steel section, thermocouple junction for the probe is located flush to the duct flow surface. The wires of the thermocouple are taken out through 6.35 mm diameter blind hole located in the respective position of the thermocouple in the top wall. These probes can measure the unperturbed temperature for long time.

Computational Methodology

Three-dimensional Reynolds Averaged Navier Stokes (RANS) equations along with species and turbulence transport equations are solved using computational flow code CFX [17]. The CFX-code is an integrated software system capable of solving diverse and complex multidimensional fluid flow problems. The code is fully implicit, finite volume method with finite element based discretization of geometry. The method retains much of the geometric flexibility of finite element methods as well as the important conservation properties of the finite volume method. It utilizes numerical upwind schemes to ensure global convergence of mass, momentum, energy and species. It implements a general non-orthogonal, structured and unstructured, boundary fitted grids. Convective terms are discretized through 2nd order spatial scheme to capture the flow features accurately. The turbulence closure was solved using *k*-ω [18] model along with wall functions.

Governing Equations

The system of equations for turbulent compressible gas may be written as,

Continuity equation:

$$\frac{\partial \rho}{\partial t} + \frac{\partial}{\partial x_k}(\rho u_k) = 0 \quad k = 1, 2, 3$$

Momentum equation:

$$\frac{\partial}{\partial t}(\rho u_i) + \frac{\partial}{\partial x_k}(\rho u_i u_k) + \frac{\partial p}{\partial x_i} = \frac{\partial(\tau_{ik})}{\partial x_k}, \quad i, k = 1, 2, 3$$

Energy equation:

$$\frac{\partial}{\partial t}(\rho H) + \frac{\partial}{\partial x_k}(\rho u_k H) = -\frac{\partial}{\partial x_k}(u_j \tau_{jk}) + \frac{\partial q_k}{\partial x_k}, \quad j, k = 1, 2, 3$$

Where, ρ, u_i, p, H are the density, velocity components, pressure and total enthalpy respectively. Turbulent shear stress is defined as

$$\tau_{ik} = \mu \left(\frac{\partial u_i}{\partial x_k} + \frac{\partial u_k}{\partial x_i} \right)$$

$\mu = \mu_l + \mu_t$ is the total viscosity; μ_l , μ_t being the laminar and turbulent viscosity. Laminar viscosity (μ_l) is calculated from Sutherland law as

$$\mu_l = \mu_{ref} \left(\frac{T}{T_{ref}} \right)^{3/2} \left(\frac{T_{ref} + S}{T + S} \right)$$

Where, T is the temperature and μ_{ref}, T_{ref} and S are known coefficient. In eddy viscosity models, the stress tensor is expressed as a function of turbulent viscosity (μ_t). Based on dimensional analysis, few variables (k, ε, ω) are defined as given below:

Turbulent kinetic energy (k) is defined as following expression, $k = \overline{u_i' u_i'}/2$ and Specific dissipation rate (ω) is defined as, $\omega \approx \frac{\varepsilon}{k}$

Where Turbulent dissipation rate (ε) is defined as,

$$\varepsilon \equiv \nu \overline{\frac{\partial u_i'}{\partial x_j} \left(\frac{\partial u_i'}{\partial x_j} + \frac{\partial u_j'}{\partial x_i} \right)}$$

The heat flux, q_k is calculated as, $q_k = -\lambda \frac{\partial T}{\partial x_k}$, λ is the thermal conductivity.

k-ω Turbulence Model

The turbulent viscosity is calculated as function of k and ω [18].

$$\mu_t = f\left(\frac{\rho k}{\omega}\right)$$

Turbulent Kinetic energy (k) equation:

$$\frac{\partial}{\partial t}(\rho k) + \frac{\partial}{\partial x_i}(\rho\, k\, u_i) = \frac{\partial}{\partial x_j}\left(\Gamma_k \frac{\partial k}{\partial x_j}\right) + G_k - Y_k$$

Specific Dissipation Rate (ω) equation:

$$\frac{\partial}{\partial t}(\rho\omega) + \frac{\partial}{\partial x_i}(\rho\, \omega\, u_i) = \frac{\partial}{\partial x_j}\left(\Gamma_\omega \frac{\partial \omega}{\partial x_j}\right) + G_\omega - Y_\omega$$

Where, G_k, Y_k, Γ_k and $\mathbf{G}_\omega$, Y_ω, Γ_ω are the production, dissipation and diffusion terms of the k and ω equations respectively.

Species Transport Equation

Conservation of Species Mass Fraction (Y_I):

$$\frac{\partial}{\partial t}(\rho\, Y_I) + \frac{\partial}{\partial x_k}(\rho\, u_k\, Y_I) = \frac{\partial}{\partial x_k}\left(\left(\frac{\mu_l}{\mathrm{Pr}} + \frac{\mu_t}{\sigma_c}\right)\frac{\partial Y_I}{\partial x_k}\right) + S_I$$

Where the source term S_I is due to the chemical reaction rate involving species component I, and Y_I is the mass fraction of I^{th} species. The chemical reactions can be described in terms of elementary reactions involving N_C components that can be written as:

$$\sum_{I=A,\,B,\,C,\,\ldots}^{N_C} v_{kI}^{i} I \qquad \leftrightarrow \sum_{I=A,\,B,\,C,\,\ldots}^{N_C} v_{kI}^{i\,i}\, I$$

where, v_{kI} is the stiochiometric coefficient for species component I in the elementary reaction k. The rate of production/consumption, S_I, for species component I can be computed as the sum of the rate of progress for all the elementary reactions in which component I participates:

$$S_I = M_I \sum_{k=1}^{K} (v_{kI}'' - v_{kI}')\, R_k$$

Where, W_I is molecular weight of species component I and R_k is the elementary reaction rate of progress for reaction, which can be calculated using Eddy Dissipation combustion model.

Combustion Modeling

Eddy dissipation combustion model is used for its simplicity and robust performance in predicting reactive flows. The model is based on the concept that chemical reaction is fast relative to the transport process in the flow. When, reactants mix at the molecular level they instantaneously form products. The model assumes that the reaction rate may be related directly to the time required to mix reactants at molecular level. In turbulent flows, this mixing time is dictated by the eddy properties and therefore the burning rate is proportional to the rate at which turbulent kinetic energy is dissipated i.e., reaction rate ~ ε/k, where k is the turbulent kinetic energy and ε is its rate of dissipation. The chemistry of the combustion reaction is represented on a mass basis by:

$$H_2 + 0.5\,(O_2 + 0.879H_2O + 2.429N_2) \rightarrow 1.439H_2O = 1.214N_2$$

The mixing rate determined from the Eddy Dissipation Model (EDM) is given as

$$R_k = -A_{ebu}\,\bar{\rho}\,\frac{\varepsilon}{k}\,\min\left\{Y_f, \frac{Y_o}{v_s}, B_{ebu}\,\frac{Y_p}{1+v_s}\right\}$$

Where, Y_f, Y_o and Y_p are the mass fractions of fuel, oxidizer and products respectively, A_{ebu} and B_{ebu} are the model constants and v_s is the stiochometric ratio.

Conjugate Heat Transfer (CHT) Method

The computational domain of a CHT problem consists of fluid domain and solid domain. In fluid domain, the three dimensional Navier-Stokes equations are solved for velocity components, pressure, density, temperature etc. In the CHT solid domain, diffusion is the only transport process, and only the energy equation is solved for temperature. The fluid energy and the solid energy equations are coupled for the identical conditions of temperature and heat flux at the solid-fluid interface.

Gas-Solid Interface Boundary Condition

For CHT approach, in general, at the gas-solid and solid-solid interface, the energy balance is done using FFTB method (Flux Forward, Temperature Backward). At the interface of two different regions the heat flux and the temperature must be conserved.

$$T_1 \mid_{\partial_{1-2}} = T_2 \mid_{\partial_{2-1}}$$

$$k_1 \frac{\partial T_1}{\partial n} \mid_{\partial_{1-2}} = k_2 \frac{\partial T_2}{\partial n} \mid_{\partial_{2-1}}$$

This is achieved using an inner iterative loop. The boundary heat flux at the common interface in the second domain is prescribed equal to the calculated heat flux in the first domain (Flux Forward). With this Neumann boundary condition, the temperature distribution on the second domain can be computed. The temperature profile obtained in the second domain at the common interface is prescribed back to the first domain as a Dirichlet boundary condition (Temperature Back). The temperature distribution and the heat flux are then computed in the first domain and the loop is iterated till the temperature and heat flux differences at the domain interface are below the desired numerical error. When the convergence is reached, the physical time step is incremented and iteration for the next time step starts. The time step for the numerical simulation is calculated based on method that the thermal pulse within the solid materials should not cross more than one computational cell within a prescribed time step. This is calculated as,

$$\delta t = \frac{\delta x^2}{2\alpha}$$

Where, δt is the time step, δx is the smallest cell characteristic length in the solid domain and α is thermal diffusivity of the solid materials.

Discretization of Governing Equations

The CFD solver utilizes a finite volume approach, in which the conservation equations are integrated over a control volume described around a node, to obtain an integral equation. The pressure integral terms in the momentum integral equation and the spatial derivative terms in the integral equations are evaluated using finite element approach. An element is described with eight neighbouring nodes. The advective term is evaluated using upwind differencing with physical advection correction. The set of discretized equations form a set of algebraic equations: $A\vec{x} = b$ where, $\vec{x}$ is the solution vector. The solver uses an iterative procedure to update an approximated x_n (solution of x at n^{th} time level) by solving for an approximate correction x' from the equation $A\vec{x}' = \vec{R}$, where $\vec{R} = \vec{b} - A\vec{x_n}$ is the residual at n^{th} time level. The equation $A\vec{x}' = \vec{R}$ is solved approximately using an approach called Incomplete Lower Upper factorization method. An algebraic multi-grid method is implemented to reduce low frequency errors in the solution of the algebraic equations. Maximum residual $(= \varphi_j^{n+1} - f(\varphi_j^{n+1}, \varphi_j^n)) < 10^{-4}$ is taken as convergence criteria. Transient simulation is performed with a time step of 1 millisecond with 40 inner co-loop iterations to get the convergence at each time step. The transient simulations are carried out for a total time of 24 seconds (initial 5.4 sec is nonreacting and remaining is reacting flow). High performance computing (HPC) cluster with 256 core with 250 GB RAM 3.0 GHz speed is used for the simulation and it takes about 20 days to complete one simulation.

Results and Discussion

Computational Domain and Grid

Both facility nozzle and combustor with fuel injection system are simulated simultaneously to predict correctly the boundary layer growth at the combustor entrance. Taking advantage of the symmetry along the width, only one half of the geometry is considered. The origin is taken at the centre of the facility nozzle exit. *X*-axis is considered along the length of the combustor, while *Y* and *Z*-axes are taken along the height and width of the combustor respectively. A structured grid of 3.6 million cells is generated using ICEM-CFD 14.5 [19]. The grid structure of the nozzle and in the neighborhood of the injector is shown in Fig.2. The grids are made sufficiently fine to capture all the flow features. To enable accurate prediction of wall heat flux, grids are taken very fine near the wall ($y^+ \sim 1$) and relatively coarser in the core.

Boundary Conditions

As the inflow is subsonic at the entry to the facility nozzle, total pressure (0.77 MPa) and total temperature (1828 K, same as experimental condition) are prescribed in the inflow plane of facility nozzle. Oxygen and water mass fractions are taken as 0.2321 and 0.2041 respectively, whereas the rest of the species mass fraction is balanced to N_2. Supersonic outflow boundary is specified at the combustor outlet. The water cooled walls of facility nozzle are considered isothermal at 500 K [20] temperature along with no slip wall condition. The inflow turbulent intensity is fixed as 25% and the ratio of turbulent to molecular viscosity is taken as 600 [20]. Both adiabatic and natural convection boundary conditions are applied at

the outer walls of copper and steel blocks in separate simulations to see the effect of exterior wall boundary condition.

Reacting Flow Simulation without CHT Analysis

Few numerical simulations of this experiment have already been reported in literature [20-24]. A reference reacting flow simulation with isothermal boundary condition is carried out to understand complex mixing, combustion and heat transfer process in the combustor and to compare the computed flow field with experimental and other numerical results. The exit plane solution of the facility nozzle provides values of various flow variables at combustor entry plane. The calculated nozzle-exit pitot pressure profiles in vertical center plane and horizontal center plane show very good agreement with the experimental data. Average values of Mach number, static pressure and static temperature are found to about 1.95, 1.05 bar and 1200 K respectively. Non-reacting simulation is carried out for initial 5.4 seconds (from 1 sec to 6.4 sec instance), while reacting simulation is carried out for rest 17.6 sec (from 6.4 to 24 sec instance). Due to use of infinitely fast rate chemistry, the reaction occurs instantaneously as soon as the oxidiser and fuel mix together. Temperature contour plots at different axial locations are shown in Fig.3. Due to use of fast chemistry, the heat release in the present computation is instantaneous whereas experimental (CARS) measurements indicate that heat-release occurs after 0.4 m. Fig.4 shows the comparison of bottom wall surface pressure between present computation, experimental data and VULCAN simulation [20]. It is to be noted that VULCAN used Drumnond's 9 species 18-reaction mechanism [21] H_2 - Air kinetics whereas an infinitely fast chemistry is used in the present computation. The instantaneous high heat release due to fast chemistry model in the present simulation is responsible for high pressure in the near injection zone. In the downstream region of combustor ($X > 0.6$ m), the present computations match better with the experimental result.

CHT Simulation for Nonreacting and Reacting Flows

The Conjugate Heat Transfer analysis is performed using both constant (Table-1) and variable material properties [25] of copper and steel block. Solid temperatures were initialized corresponding to the reported measured data at 1 sec which are 335 K and 365 K for copper and steel blocks respectively. Non-reacting CHT simulation is carried out for 5.4 sec before fuel injection while reacting flow CHT simulation has been carried out for next 17.6 seconds with fuel injection. Outside wall was assumed adiabatic in the simulation. The transient wall temperature is monitored at locations, 2.8 mm from the interface for copper block and adjacent to interface for steel block. Comparison of temperature history with time at three locations on top wall is shown in Figs.5 (a) to (c) respectively. Simulation results with variable material properties are also shown in the same figure. The density of material which does not vary much with temperature is taken as constant (Table-1), while the variations of specific heat (C_p) and thermal conductivity (k) are taken as a function of temperature [25]. In the zone of interest, the values of specific heat (C_p) and thermal conductivity (k) for copper vary less than 5.6% and 5.0% respectively in the temperature range of 300 K to 600 K, whereas, the same parameters vary about 82% and 48% respectively for carbon steel in the temperature range of 300 K to 900 K. It is observed that present CFD over predicts the experimental results in the copper block (10 % and 6 % near at X=197 mm and X=426 mm respectively). More heat release due to infinitely fast chemistry assumptions may be the cause for the over prediction of the results adjacent to the injection zone. In the downstream location in steel block, CFD under predicts the experimental data (maximum difference is 12% at X=978 mm). Early completion of the reaction in the present simulation is conjectured to be the reason for the under-prediction at the downstream locations. Temperature dependent material properties have marginal effect on interface wall temperature prediction. Since the duct is uncooled, temperatures vary greatly in the solids during the course of the run. Temperature distribution for both fluid and solid domain in X-Y plane at mid-width of the combustor is shown in Fig.6a for time t = 24 seconds. Solid temperature distribution in local scale is shown in Fig.6b. In the copper section, temperature rises from 335 K at the start (1 sec instance) to as high as 550 K at the end of 24 seconds. In the carbon steel section, it varies from 365 K at the start (1 sec instance) to as high as 905 K at the end of the test time.

Table-1 : Properties of Materials

Material	Density, ρ (kg/m^3)	Specific Heat, C_p (J/kg-K)	Thermal Conductivity, k (W/m-K)
Copper	8933	385	401
Steel	7854	434	60.5

A separate simulation has been carried out with natural convection heat transfer exterior boundary condition for

copper and steel block. The results of the simulation are compared with adiabatic wall boundary condition (along with experimental results) at X=426 mm and are shown in Fig.7. Almost identical results have been achieved for both the simulations, showing minimal effect of wall exterior boundary condition.

The temperature distribution inside the copper and steel block along the thickness (from inner wall surface to outer wall surface) at t = 24 sec are shown in Fig.8. The effect of variable properties is negligible for copper section (variation in temperature is less than 1%) because the material property variation is minimal for the copper section; while it is significant for the steel section. Predicted outer wall temperature in case of variable property is about 10.0% less compared to constant wall property case.

Figure 9(a) shows the axial distribution of inner and outer wall surface temperature comparison for both the blocks. The difference of both the wall surface temperature at a particular X location is less in copper block compared to the steel block because heat conduction in copper is faster than steel due to higher thermal conductivity of copper. Fig.9(b) shows inner wall heat flux distribution along the X-axis of the combustor top wall. The heat flux is maximum adjacent to the injection region, as more heat release occurs just after fuel injection due to fast chemistry assumption. In the downstream, it reduces due to lesser heat release from combustion and expansion of combustion gas in divergent section. Fig.10 gives the interface temperature along the combustor bottom wall at different time instants. The temperature for copper section is 335 K and for steel section, initial (at t = 1 sec) temperature increases from 365 K. For reacting flow, the rate of temperature increase is more initially which decreases gradually with time towards the end of the experiment.

Conclusions

Numerical simulations were carried out for SCHOLAR scramjet combustor to explore the CHT capability of CFX code in reacting flow. CHT analysis is performed for 23 seconds to predict the transient wall temperature. The facility nozzle is modeled along with combustor to provide realistic inflow conditions for the combustor. Computed thermochemical variables match reasonably well the experimental and other numerical data. It is observed that the wall temperature is over predicted (maximum 10%) for the locations near the combustion zone while it is under predicted (12%) for the location away from the reaction zone. High heat release near the injector due to fast chemistry (EDM) combustion model and early completion of the reaction are conjectured to be the cause of over prediction in the forward portion and underprediction in the rearward portion respectively. The variable material properties and the natural convection boundary condition for the copper and steel block have negligible effect on interface wall temperature prediction. But it affects the temperature distribution inside solid region significantly.

References

1. Manna, P. and Debasis Chakraborty., "Numerical Investigation of Conjugate Heat Transfer Problems", Journal of Aerospace Sciences and Technologies, Vol.56, No.3, 2004, pp.166-175.

2. Chandramurty, M.S.R., Manna, P. and Debasis Chakraborty., "Conjugate Heat Transfer Analysis in High Speed Flows", Journal of Aerospace Engineering, Vol.227, No.10, 2013, pp.1672-1681.

3. Marineau, E.C., Schetz, J.A. and Neel, R.E., "Turbulent Navier-Stokes Simulations of Heat Transfer with Complex Wall Temperature Variations", AIAA Paper No. 2006-3087, 2006.

4. GASP 4.0 User Manual, AeroSoft, ISBN 09652780-5-0, 2002.

5. Back, L.H., Massier, P.F. and Gier, H.L., "Conjugate Heat Transfer in a Convergent-Divergent Nozzle", NASA TR 32-415.

6. Aydin, O., Avci, M., Bali, T. and Arici M.E.,"Conjugate heat transfer in a Duct with an Axially Varying Heat Flux", International Journal of Heat and Mass Transfer, Vol.76, 2014, pp.385-392.

7. Engblom, W.A., Fletcher, B. and Georgiadis, N.J., "Validation of Conjugate Heat Transfer Capability for Water-Cooled High-Speed Flows", AIAA Paper No.2007-4392, 2007.

8. Nelson, C.C. and Power, G.D., "CHSSI Project CFD-7: The NPARC Alliance Flow Simulation System", AIAA Paper No. 2001-594, 2001.

9. Engblom, W. and Goldstein, D., "Nose-Tip Surface Heat Reduction Mechanism", AIAA Journal of Ther-

mophysics and Heat Transfer, Vol.10, No.4, 1996, pp.598-606.

10. Matthew, E.F. and Davis, R.L., "A Conjugate Heat Transfer RANS/DES Simulation Procedure", AIAA Paper No. 2009-913, 2009.

11. Davis, R.L. and Dannenhoffer, J.F., "Detached Eddy Simulation Procedure Targeted for Design", AIAA Journal of Propulsion and Power, Vol.24, No.6, 2008, pp.1287-1294.

12. Chandramurty, M.S.R. and Debasis Chakraborty., "Thermal Response Analysis of Scramjet Combustor Wall to High Speed Turbulent Reacting Flow, Science, Technologies, and Industry Practice in Aerodynamics and Design", Proceedings of SAROD-2009, held at Bangalore on December 10-12, 2009, pp.698-710.

13. Cutler, A.D., Danehy, P.M., Springer, R.R., DeLoach, R. and Capriotti, D.P.,"CARS Thermometry in a Supersonic Combustor for CFD Code Validation", AIAA Paper No.2002-0743, 2002.

14. Cutler, A.D., Diskin, G.S., Danehy, P.M. and Drummond, J.P., "Fundamental Mixing and Combustion Experiments for Propelled Hypersonic Flight", AIAA Paper No.2002-3879, 2002.

15. Cutler, A.D., Danehy, P.M., O'Byrne, S., Rodriguez, C.G. and Drummond, J.P., "Supersonic Combustion Experiments for CFD Model Development and Validation" (Invited), 42nd AIAA Aerospace Sciences Meeting and Exhibit, 5-8 January 2004, Reno, Nevada, AIAA Paper No.2004-266.

16. Rust, B., Gerlinger, P., Jean-Michel, L., Kindler, M. and Aigner, M., "Numerical Simulation of the Internal and External Flowfields of a Scramjet Fuel Strut Injector Including Conjugate Heat Transfer", AIAA Paper No.2011-2207, 2011.

17. ANSYS-CFX, Version-14.5, Release and Installation, January, 2013.

18. Wilcox, D.C., "Multiscale Model for Turbulent Flows", AIAA Journal, Vo.26, No.11, 1988, pp.1311-1320.

19. ANSYS, ICEM-CFD-14.5, Installation and Overview, January, 2013.

20. Rodriguez, C.G. and Cutler, A.D., "CFD Analysis of the Scholar Scramjet Model", AIAA Paper No.2003-7039, 2003.

21. Drummond, J.P., "A Two-Dimensional Numerical Simulation of a Supersonic, Chemically Reacting Mixing Layer", NASA TM 4055, 1988.

22. Ingenito, A. and Bruno, C.,"LES of a Supersonic Combustor with Variable Turbulent Prandtl and Schmidt Numbers", AIAA Paper No.2008-0515, 2008.

23. Ingenito, A. and Bruno, C. , "Reaction Regime in Supersonic Flows", AIAA Paper No.2009-0812, 2009.

24. Chandramurty, M.S.R. and Debasis Chakraborty., "Numerical Simulation of Angular Injection of Hydrogen Fuel in Scramjet Combustor", Journal of Aerospace Engineering, Vol.226, No.7, 2012, pp.861-872.

25. www.mace.manchester.ac.uk/project/research/structures/strucfire/materialInFire/steel/ Hot RolledCarbonSteel/thermalProperties.html.

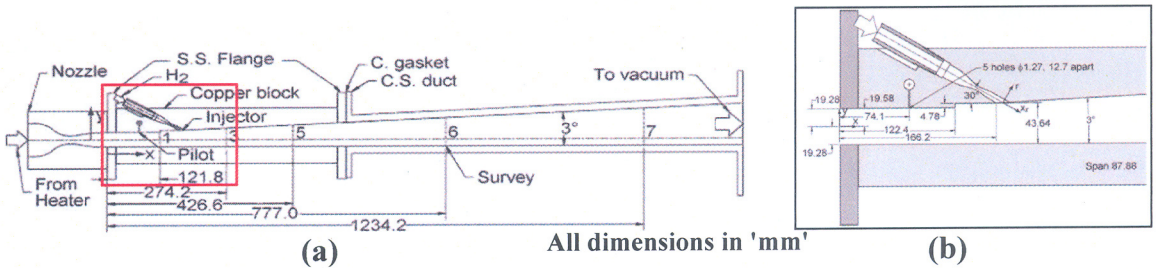

Fig.1 SCHOLAR Combustor Model (a) Facility Nozzle, Copper and Steel Duct Sections (b) Zoomed View in the Vicinity of Fuel Injector and Pilots

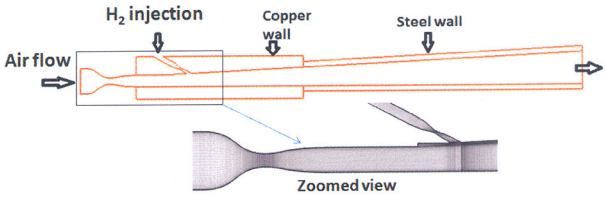

Fig.2 Computational Domain of SCHOLAR Combustor with Grid Near Injector Region

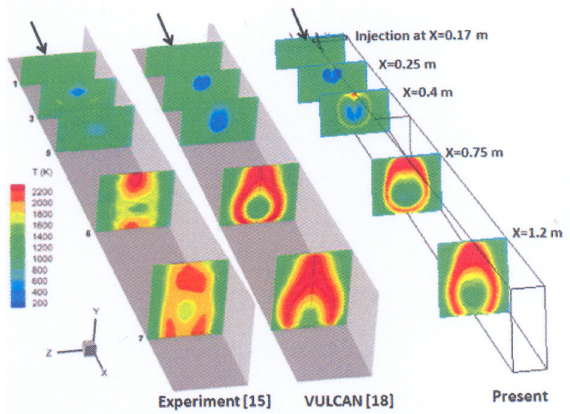

Fig.3 Temperature Distribution Comparison at Various Cross Sections Between Experiment, VULCAN and Present Simulation

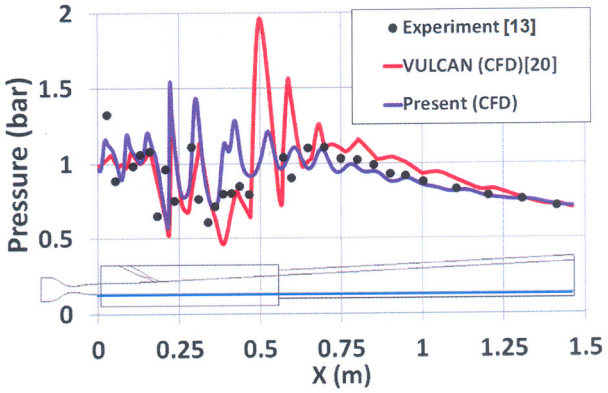

Fig.4 Comparison of Centerline Bottom Wall Pressure Distribution

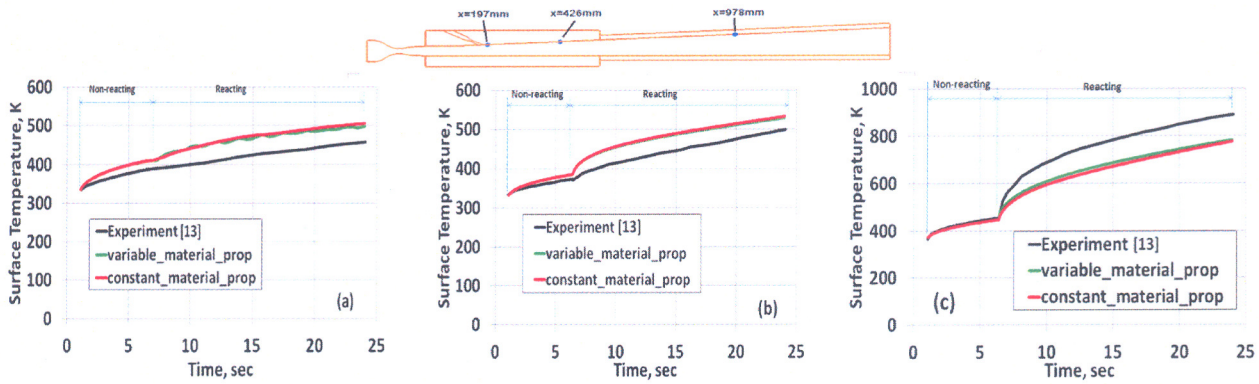

Fig.5 Comparison of Transient Wall Temperature at (a) X = 197 mm (b) X = 426 mm and (c) X = 978 mm

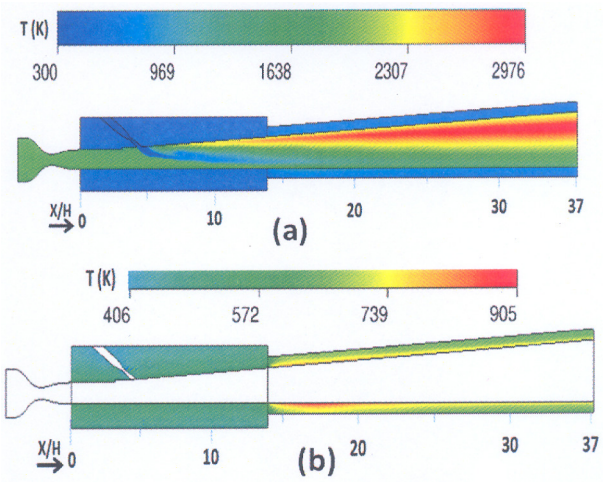

Fig.6 Temperature Distribution in X-Y Plane (Z = 0)
(a) Fluid-Solid Zone (Global Scale)
(b) Solid Zone Alone (Local Scale)

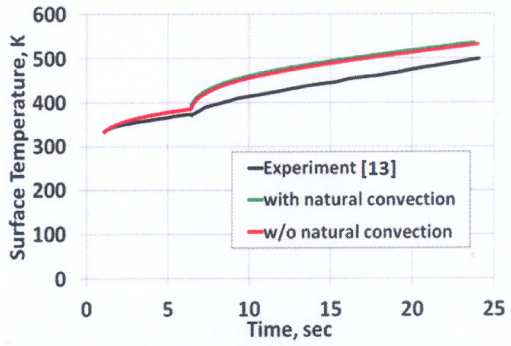

Fig.7 Comparison of Transient Wall Temperature at X = 426 mm

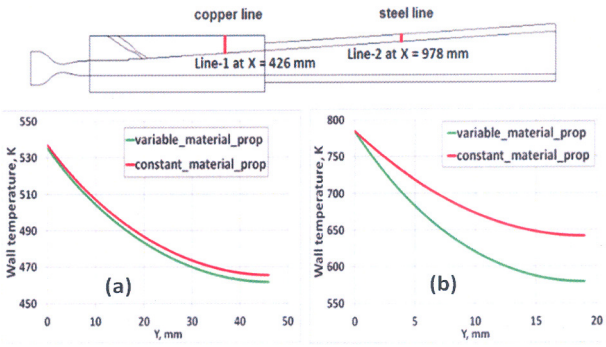

Fig.8 Comparison of Temperature Distribution in Solid at t = 24 sec (a) Along Line-1 at X = 426 mm
(b) Along Line-2 at X = 978 mm

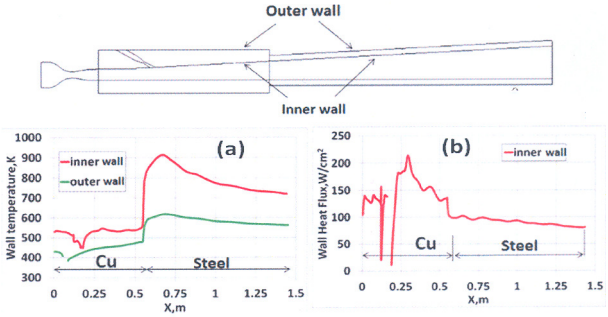

Fig.9 Temperature and Wall Heat Flux Along Combustor Wall at 24 sec (a) Surface Temperature Comparison (b) Heat Flux Distribution

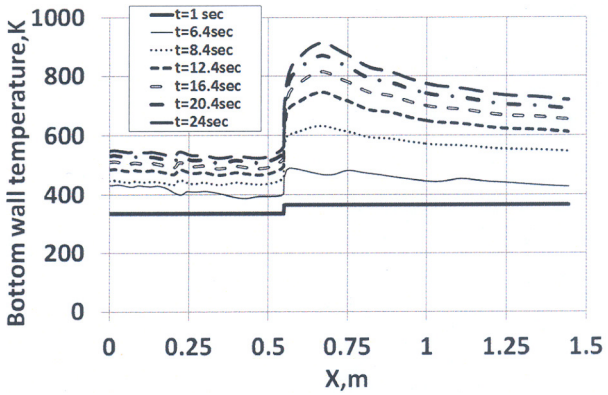

Fig.10 Centreline Bottom Wall Interface Temperature at Different Time Instants